

## Effects of tip-gap size on the tip-leakage flow in a turbomachinery cascade

Donghyun You<sup>a)</sup>

*Center for Turbulence Research, Stanford University, Stanford, California 94305*

Meng Wang

*Department of Aerospace and Mechanical Engineering, University of Notre Dame, Notre Dame, Indiana 46556*

Parviz Moin

*Center for Turbulence Research, Stanford University, Stanford, California 94305*

Rajat Mittal

*Department of Mechanical and Aerospace Engineering, George Washington University, Washington, D.C. 20052*

(Received 23 May 2006; accepted 15 August 2006; published online 5 October 2006)

The effects of tip-gap size on the tip-leakage vortical structures and velocity and pressure fields are investigated using large-eddy simulation, with the objective of providing guidelines for controlling tip-leakage cavitation and viscous losses associated with the tip-leakage flow. The effects of tip-gap size on the generation and evolution of the end-wall vortical structures are discussed by investigating their evolutionary trajectories and the mean velocity field. The tip-leakage jet and tip-leakage vortex are found to produce significant mean velocity gradients, leading to the production of vorticity and turbulent kinetic energy. Inside the cascade passage, the peak streamwise velocity deficit and magnitudes of vorticity and turbulent kinetic energy in the tip-leakage vortex are reduced as the tip-gap size decreases. The present analysis indicates that the mechanisms for the generation of vorticity and turbulent kinetic energy are mostly unchanged by the tip-gap size variation. However, larger tip-gap sizes are found to be more inductive to tip-leakage cavitation judged by the levels of negative mean pressure and pressure fluctuations. © 2006 American Institute of Physics. [DOI: 10.1063/1.2354544]

### I. INTRODUCTION

The radial clearance between a rotor-blade tip and casing wall in a turbomachine is indispensable for its operation. However, its existence has been a major source of unfavorable flow phenomena. Complicated vortical structures are generated by the tip-clearance flow and its interactions with the end-wall boundary layer, the blade wake, and neighboring blade. The tip-clearance vortical structures often induce rotating instabilities and blockage in the flow passage which result in severe performance loss and subsequent stall of axial compressors.<sup>1,2</sup> In a transonic compressor, interaction between passage shock and tip-clearance flow is implicated in the degradation of efficiency as well as vibrations and noise generation<sup>3</sup> while tip-leakage cavitation is induced by the low pressure events in the vicinity and downstream of the tip gap of liquid pumps.<sup>4–8</sup> These issues have motivated a number of experimental and computational investigations where a reduction of the tip-clearance flow related detrimental effects was attempted through the change of tip-gap size.<sup>4–14</sup>

In axial compressors, it has been reported that an increase of tip gap between the blade tip and casing wall also increases the size of the tip-leakage vortex and shifts the origin of the vortex further downstream with an increased

angle between the path of the tip-leakage vortex center and that of the blade wake.<sup>9,10</sup> Storer and Cumpsty<sup>11</sup> employed a compressor cascade with a variety of tip-gap sizes and showed a nonlinear relation of total pressure loss with the tip-gap size, while the size of tip-leakage vortex varied linearly with tip-gap height. Later experimental studies by Zierke *et al.*<sup>4</sup> and Zierke and Straka<sup>5</sup> in a high-Reynolds-number pump facility showed that the size of the rotor tip gap significantly influences the evolution of the tip-leakage vortex and resultant cavitation.

The effects of tip-gap size on the tip-leakage cavitation in a rotating hydraulic pump were examined more extensively by Farrell and Billel<sup>6</sup> who found that the cavitation inception indices increase with decreasing tip-gap sizes. They also found a minimum in the cavitation inception index when the ratio of tip-gap size to the maximum tip thickness is in the range of 0.1–0.2. Experiments performed by Boulon *et al.*<sup>7</sup> in a setup with a stationary end-wall showed decreased cavitation inception indices with decreasing tip-gap sizes. Similar observations were reported by Gopalan *et al.*<sup>8</sup> Although the gross effects of tip-gap size on the tip-leakage flow have been known for sometime, the quantitative effects on the dynamics of the tip-leakage vortical structures, tip-leakage cavitation, and performance loss associated with the tip-leakage flow are poorly understood.

In recent experiments performed at Virginia Tech, which are also benchmarked in the present large eddy simulation

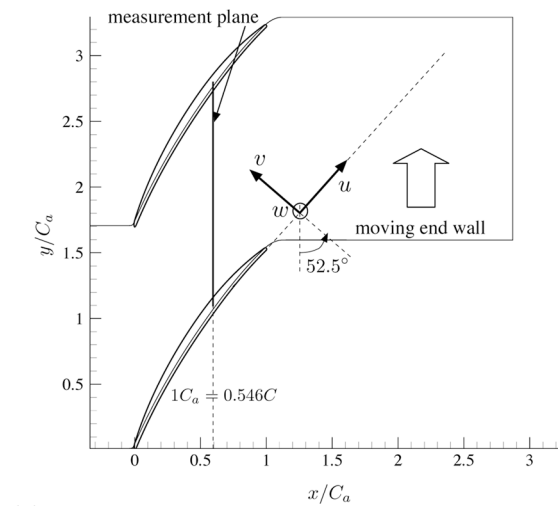
<sup>a)</sup> Author to whom correspondence should be addressed. Telephone: +1-650-725-1821. Fax: +1-650-725-3525. Electronic mail: [dyou@stanford.edu](mailto:dyou@stanford.edu)

(LES) study, the effects of tip-gap size on the downstream tip-leakage flow field were examined.<sup>12,13</sup> Since the experiments were performed in a wind tunnel, cavitation was not an issue in those studies. Muthanna and Devenport<sup>12</sup> investigated the effects of tip-gap size on the cross-sectional structure of the tip-leakage vortex at about three axial chord ( $C_a$ ) lengths downstream from the trailing-edge by comparing the mean flow and turbulence properties in the base tip-gap size (3.06% axial chord) with those in the doubled and halved tip-gap sizes. The vortex center, defined by the location of peak streamwise vorticity, moved across the end-wall and the pitchwise separation between the vortex and wake center increased as the tip gap was increased. In general, the regions of tip-leakage flow in terms of mean velocity, vorticity, and turbulent kinetic energy were found to increase in size as the tip gap size increased. However, the magnitudes of streamwise mean velocity deficit and turbulent kinetic energy in the downstream tip-leakage vortex appeared to be almost unchanged by the tip-gap size variation. Wang and Devenport<sup>13</sup> performed experiments in the same configuration studied by Muthanna and Devenport<sup>12</sup> but replaced the stationary end-wall with a moving end-wall. Many of the characteristics of the tip-leakage vortex including the mechanism that drives the vortex were similar to those observed without end-wall motion.

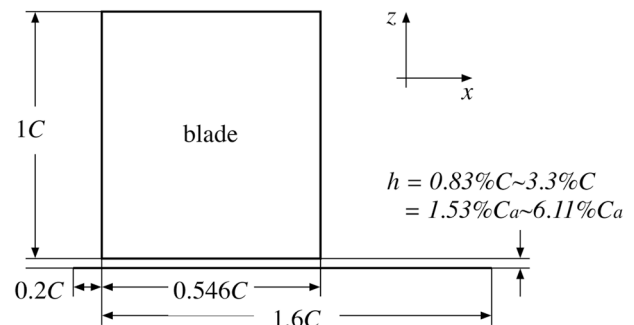
However, these studies<sup>12,13</sup> focused on the flow field downstream of the cascade passage and did not provide information regarding the effects of tip-gap size on the generation and evolution stages of the tip-leakage vortex and other induced (scraping) or tip-separation vortices. In addition, the previous experimental<sup>12,13</sup> and Reynolds-averaged Navier-Stokes (RANS) computational studies<sup>15,16</sup> could not provide information regarding the unsteady pressure field in the cascade passage region. Since the induced and tip-separation vortices, as well as the tip-leakage vortex, can significantly influence the tip-leakage cavitation phenomenon, detailed effects of tip-gap size on the vortical structures need to be better understood. An understanding of the effects of tip-gap size on the pressure field in the vicinity of the tip gap is also crucial in designing cavitation-control methodologies based on the optimal tip-gap size or on modifications of the blade tip and end-wall.

In this study, the tip-leakage flow, particularly in regions not studied experimentally,<sup>13</sup> is investigated using data obtained by LES. In Refs. 14 and 17, the mean and turbulence statistics, the vortex dynamics, and the space-time correlations of velocity and pressure fluctuations in a linear cascade configuration with a tip-gap size of 3.06% axial chord were computed, validated, and analyzed throughout the cascade passage, inside the tip gap, and at several downstream locations. This paper deals with the effects of tip-gap size on the tip-clearance flow dynamics with a particular emphasis on understanding the effects of tip-gap size on the end-wall vortex dynamics, mechanisms for viscous losses, and tip-leakage cavitation.

Flow configurations and grid spacings for the simulations are addressed in Sec. II. Results and discussion of the effects of tip-gap size on various features of the tip-



(a)



(b)

FIG. 1. Configuration for flow in a linear cascade with tip clearance and definitions of the velocity coordinates. (a) Top ( $x$ - $y$ ) view; (b) side ( $x$ - $z$ ) view.

clearance flow are given in Sec. III, followed by conclusions in Sec. IV.

## II. COMPUTATIONAL SETUP

### A. Flow configuration

The numerical algorithms and their implementation are described in Ref. 17 in detail. The three-dimensional, unsteady, incompressible Navier-Stokes equations are solved in a generalized coordinate system in conjunction with a Lagrangian dynamic subgrid-scale (SGS) model.<sup>18</sup>

The flow configuration and coordinate definitions are schematically shown in Fig. 1. The present study is focused on a linear cascade with a moving end-wall at the bottom of the tip gap, matching the experimental setup in Ref. 13. A single blade passage is considered, with periodic boundary conditions in the  $y$  direction to mimic the flow in the interior of a cascade. The computational domain is of size  $L_x \times L_y \times L_z = 3.30C_a \times 1.70C_a \times 1.83C_a$  for the three tip-gap cases.  $C_a$  is the axial chord length [see Fig. 1(a) for the definition] and its dimensional value was 138.684 mm in the experiment.<sup>13</sup>

The important parameters for the simulations are as follows: The sizes of the tip clearances ( $h$ ) are  $6.11\% C_a$ ,  $3.06\% C_a$ , and  $1.53\% C_a$ , the blade pitch is  $1.70 C_a$ , and the blade span is  $1.83 C_a$ . The blade has a relatively high stagger-angle of about  $57^\circ$ . The Reynolds number of this flow is 400 000 based on the chord ( $C=1.832 C_a$ ) and inflow free-stream velocity, and the inflow turbulent boundary layer has a Reynolds number of 780 based on the momentum thickness.

The flow downstream is highly dependent on the conditions at the inlet and makes it necessary to specify realistic turbulent fluctuations that are in equilibrium with the mean flow. The inflow turbulent boundary-layer data are provided using the method of Lund *et al.*,<sup>19</sup> modified to account for the fact that the mean flow direction is not perpendicular to the inflow/outflow plane. The computational domain size employed in the inflow generation simulation is 8 and 2 boundary layer thickness units in the streamwise and wall-normal directions, respectively, while the pitchwise domain size is identical to the pitch of the cascade. The grid distribution in the cross-stream plane ( $y$ - $z$ ) is matched to that in the tip-clearance flow simulation and the total number of mesh points for this simulation is  $64 \times 351 \times 52$  ( $x \times y \times z$ ). The grid resolution in wall-units in the streamwise and spanwise directions is less than 50 and 1, respectively. The time-step in wall-units is roughly 2.

In more realistic turbomachinery applications, the effects of pressure gradients and curvature also need to be accounted for in the inflow generation. In addition, the downstream cascade in a multirow turbomachine requires inflow consisting of the end-wall boundary layer, the upstream wake, and the end-wall vortical structures. For example, to mimic the stator-rotor interaction, You *et al.* employed vortex generators to emulate the vortical structures embedded in the end-wall boundary layer.<sup>20</sup>

No-slip boundary conditions are applied along the rotor blade and upper and lower end-walls, and a convective boundary condition is applied at the exit boundary. The difficulty in grid topology for the tip-clearance configuration is overcome by a novel approach which combines an immersed boundary technique with a structured grid in a generalized coordinate system.<sup>17</sup> In addition to this, the high stagger angle in the experimental setup necessitates the use of a significantly skewed mesh, which requires fine control of mesh parameters such as stretching ratio and aspect ratio, and an adequate formulation of nonlinear convection terms to avoid numerical instability (see Refs. 21 and 22 for more details).

## B. Grid spacing and resolution

The mesh size used for the present simulations is  $449 \times 351 \times 161$ . It is determined iteratively based on the results from the baseline ( $3.06\% C_a$ ) tip-gap simulations. Grid lines are clustered around the blade tip, blade pressure and suction surfaces, and end-wall to ensure appropriate resolution in important flow regions. 46, 36, and 30 mesh points are allocated across the tip-gap region for tip-gap sizes of  $6.11\% C_a$ ,  $3.06\% C_a$ , and  $1.53\% C_a$ , respectively.

In general, the grid resolution on the blade surface is

reasonable compared to previous LES studies of wall bounded turbulent flows using similar numerical methods.<sup>23</sup> The grid spacings based on the chord in the streamwise, pitchwise, and spanwise directions are  $9.9 \times 10^{-4} \leq \Delta x/C \leq 1.4 \times 10^{-2}$ ,  $9.8 \times 10^{-4} \leq \Delta y/C \leq 6.5 \times 10^{-3}$ , and  $4.6 \times 10^{-4} \leq \Delta z/C \leq 1.2 \times 10^{-2}$ , respectively. In wall units, the blade-surface resolution in the region of primary interest is within the range  $\Delta x^+ \leq 50$ ,  $\Delta y^+ \leq 3$ , and  $\Delta z^+ \leq 30$  ( $\Delta z^+$  increases up to 90 far from the tip-gap region). Grid resolution normal to the end-wall is in the range of  $0.3 \leq \Delta z^+ \leq 2.1$ . In the directions parallel to the end-wall,  $\Delta x^+$  and  $\Delta y^+$  are generally less than 50, except for a small end-wall region where the maximum values reach 90–100 because of the strong effect of the tip-leakage vortex on the boundary layer. It has been found that the typical end-wall vortices are reasonably well predicted with the present grid resolution. For example, in the  $y^*$ - $z$  plane at  $x^*/C_a=1.1$  (see Fig. 5 for the definition), more than 50 grid points across the tip-leakage vortex and about 10 points across the smallest vortex are allocated for the  $3.06 C_a$  tip-gap case.

Prior to this simulation, coarser grid simulations had been carried out to determine the resolution requirements, and the final mesh was subsequently constructed using this information. To investigate the grid sensitivity, simulations of flow through the cascade without tip-gap, which are less expensive than the present simulation, were performed with refined meshes in all three directions, and it was confirmed that results were relatively insensitive to the grid resolution. The grid resolution study and comparisons with experimental data were reported in Ref. 17.

The simulation is advanced in time with the maximum Courant-Friedrichs-Lewy (CFL) number equal to 4 which corresponds to  $\Delta t U_\infty / C_a \approx 1.33 \times 10^{-3}$  where  $U_\infty$  is the incoming freestream velocity. Each time-step requires a wallclock time of about 200 s when 128 CPUs of an SGI Origin 3800 are used. In wall units, the time-step is in the range of  $0.078 \leq \Delta t^+ = \Delta t u_\tau^2 / \nu \leq 3.79$ . The maximum  $\Delta t^+$  is found underneath the blade tip, and except for this location,  $\Delta t^+$  is generally less than 0.8. The results which will be discussed below are obtained by integrating the governing equations over a time interval of about  $55 C_a / U_\infty$ .

A systematic validation of the LES predictions has been conducted and reported in Refs. 14 and 17. Comparisons were made with experimental data<sup>13</sup> in terms of mean velocity and turbulence statistics in the measurement planes downstream of the trailing edge, and reasonable agreements were obtained.

## III. RESULTS AND DISCUSSION

### A. Effects on the overall flow features

Gross features of the tip-leakage vortices generated in the different tip-gap size configurations are shown in Fig. 2, which depicts isosurfaces of instantaneous negative pressure and stream traces for each tip gap. The size of the tip-leakage vortex increases as the tip-gap size increases, and its origin is delayed further downstream. The angle between the blade chord and the tip-leakage vortex also increases with the

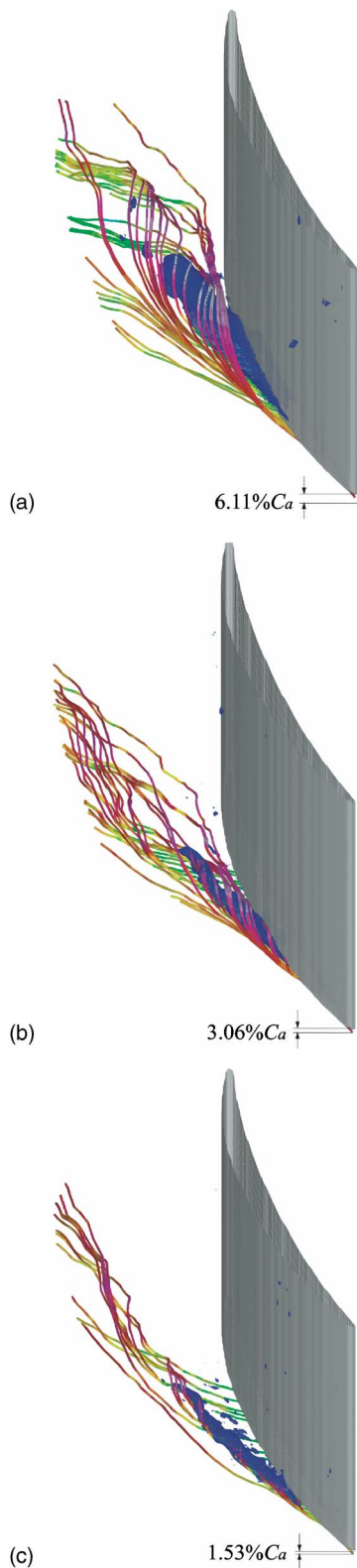


FIG. 2. Snapshots of negative pressure (blue) isosurfaces and stream traces (colored lines) showing the swirling tip-leakage flow and vortex for three different tip-gap sizes. The contour level for isosurfaces is  $p/\rho U_\infty^2 = -0.05$ . (a)  $h = 6.11\% C_a$ ; (b)  $h = 3.06\% C_a$ ; (c)  $h = 1.53\% C_a$ .

tip-gap size. Similar observations were reported by Muthanna and Devenport<sup>12</sup> and Wang and Devenport<sup>13</sup> in their experiments. Based on the size of the negative pressure region, it can be deduced that tip-leakage cavitation is more

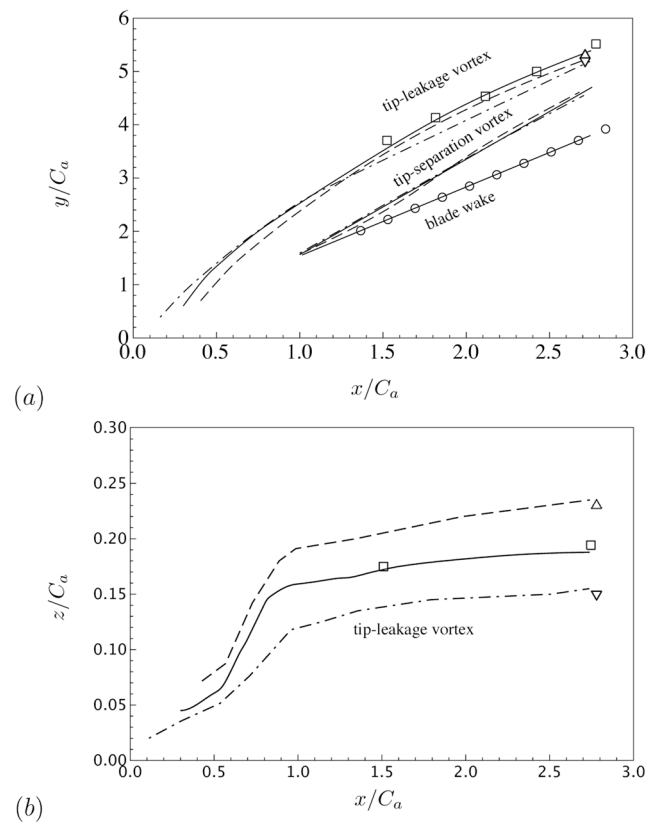


FIG. 3. Trajectories of the tip-leakage vortex, the trailing-edge tip-separation vortex, and the peak deficit of the blade wake in the linear cascades with three different tip-gap sizes along the streamwise direction. (a)  $x$ - $y$  plane; (b)  $x$ - $z$  plane. ---,  $6.11\% C_a$  tip gap; —,  $3.06\% C_a$  tip gap; - - -,  $1.53\% C_a$  tip gap; Symbols represent experimental data of Wang and Devenport (Ref. 13).

likely as the tip-gap size increases in the present configuration (Fig. 2). Detailed investigation of the effects on cavitation inception will be further discussed in Sec. III D.

Modification of tip-gap size significantly influences the trajectory of the tip-leakage vortex. In Fig. 3, the effects of the tip-gap size on the evolutions of the tip-leakage vortex, the trailing-edge tip-separation vortex, and blade wake are shown. In general, the trajectories of the tip-leakage vortex and blade wake are in favorable agreement with experimental data while the trajectories for the trailing-edge tip-separation vortex are not provided in the experiment. As already observed in the pressure isosurfaces (Fig. 2), the origin of the tip-leakage vortex is delayed further downstream from the leading edge, and the angle between the trajectory of the tip-leakage vortex and blade chord in the  $x$ - $y$  plane increases as tip-gap size increases. Although, in the  $x$ - $y$  plane, the propagation slopes of the tip-leakage vortices for the three tip gaps are different within the cascade passage, the slopes become similar downstream of the trailing edge [Fig. 3(a)]. Once the tip-leakage vortex is lifted from the end-wall, the variation of the spanwise location ( $z$ ) of the vortex is mild [Fig. 3(b)], and the resulting angle of vortex propagation in the  $x$ - $y$  plane [Fig. 3(a)] becomes similar to that of the blade wake in the downstream locations from the trailing edge since the vortex convects following the cascade main stream.

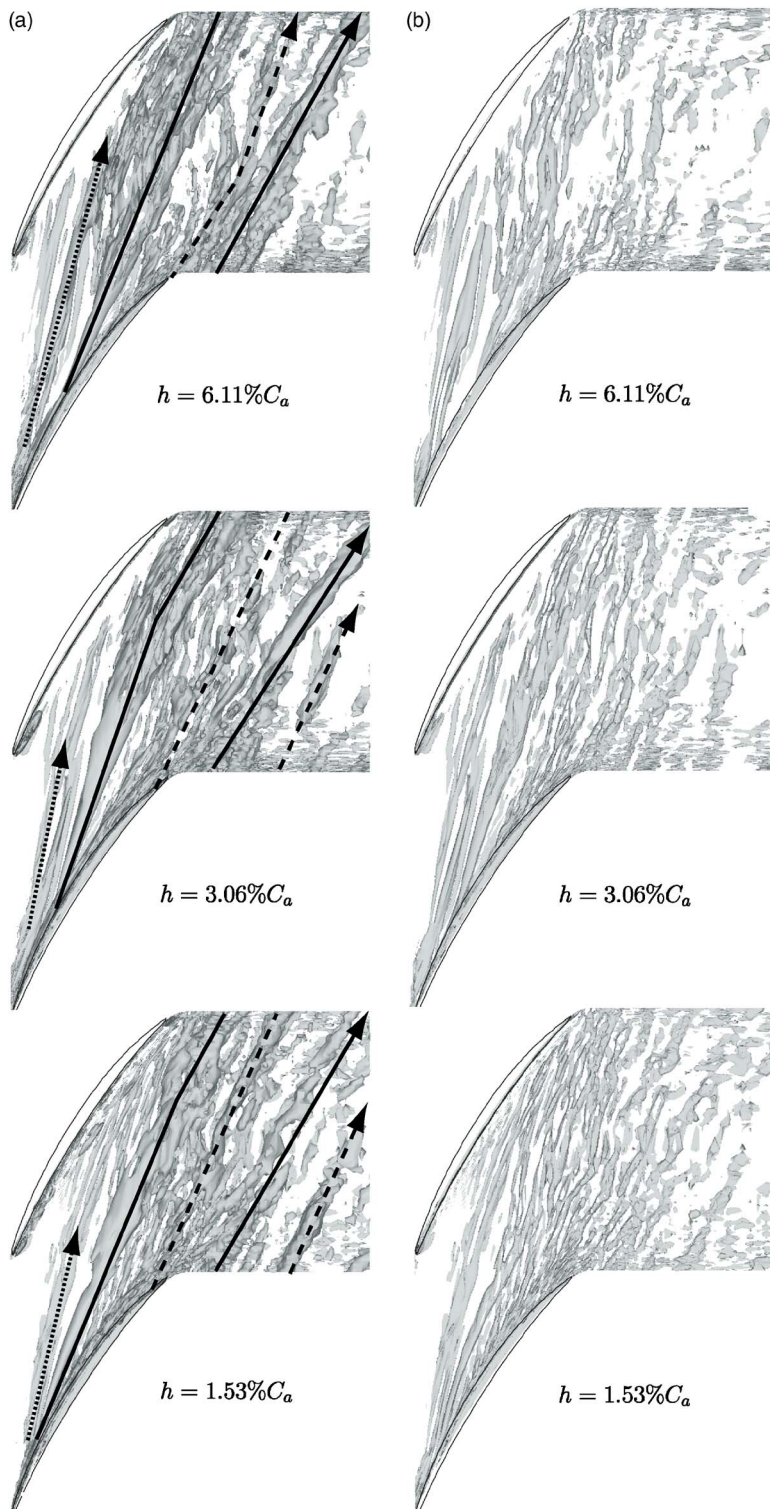


FIG. 4. Vortical structures in three tip-gap configurations visualized using the  $\lambda_2$  vortex identification method (Ref. 24). Vortical structures are shown from the top of  $x$ - $y$  planes in the range of (a)  $0 < z/C_a \leq 0.1$ ; (b)  $0 < z/C_a \leq 0.02$ , respectively. —, tip-leakage vortex; ---, trailing-edge tip-separation vortex; ···, induced vortex.

In contrast to the lifted tip-leakage vortex, the trailing-edge tip-separation vortex are driven by both the end-wall motion and the cascade main stream, resulting in a slightly higher propagation angle in the  $x$ - $y$  plane than that of the tip-leakage vortex.

### B. Effects on the vortex dynamics

The end-wall vortical structures are visualized using the  $\lambda_2$  vortex identification method<sup>24</sup> and are shown in Fig. 4. In

this vortex identification method, eigenvalues of the symmetric tensor  $S^2 + \Omega^2$ , where  $S$  and  $\Omega$  are, respectively, the symmetric and antisymmetric parts of the velocity gradient tensor, are considered. If  $\lambda_1$ ,  $\lambda_2$ , and  $\lambda_3$  are the eigenvalues and  $\lambda_1 \geq \lambda_2 \geq \lambda_3$ , the definition of a vortex in an incompressible flow is equivalent to the requirement that  $\lambda_2 < 0$  within the vortex core. The visualized end-wall vortical structures can obviously depend on their distances from the end-wall. To clarify the distinguished vortical structures, two  $x$ - $y$  planes

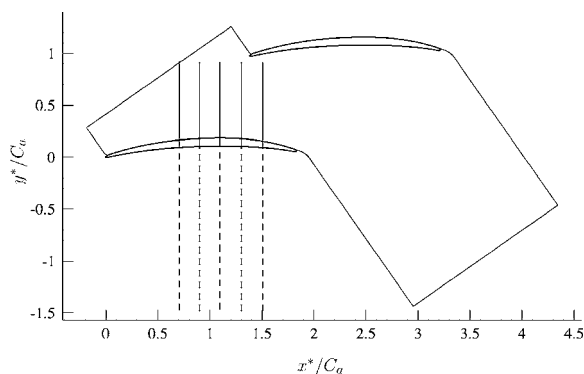


FIG. 5. Locations of the end-wall normal planes in which the mean streamlines in Fig. 6 are visualized.

with restricted spanwise domains of  $0 < z/C_a \leq 0.1$  and  $0 < z/C_a \leq 0.02$  are shown for each tip-gap size. For all three tip-gaps considered in this study, the tip-leakage vortex dominates the tip-clearance vortical structures [Fig. 4(a)]. The upstream induced vortices, which are found slightly to the left of the tip-leakage vortex, are observed to be the strongest in the bigger tip-gap (6.11%  $C_a$ ) case, and decrease in strength as the tip-gap size decreases. On the other hand, the tip-separation vortices are found to increase in numbers and strengths as the tip-gap size decreases [Fig. 4(b)].

Comparison of vortical structures in the two restricted spanwise domain sizes shows how the pitchwise end-wall motion affects the end-wall vortical structures. Vortical structures close to the end-wall evolve in the pitchwise oriented direction, and their propagation angles are clearly different from that of the tip-leakage vortex. Further downstream from the trailing edge, the tip-leakage vortex and tip-separation vortices are eventually merged by the difference between their propagation angles. Previous experiments could not reflect these features clearly due to the technical difficulty in measuring flow quantities on the moving end-wall.<sup>12,13</sup> However, very similar features of the tip-leakage vortex and tip-separation vortices were reported by Zierke *et al.*<sup>4</sup> and Zierke and Straka,<sup>5</sup> who observed a tip-separation vortex originated from the suction side of the blade tip near the trailing edge (they called the vortex a trailing edge vortex). In their axial hydraulic pump facility, the tip-separation vortex was observed to propagate along the circumferential (pitchwise) direction and to merge into the tip-leakage vortex, which convects in the axial direction, further downstream from the trailing edge.

Although the  $\lambda_2$  vortex identification method can provide the size of the vortical motion, it cannot provide the direction of the vortex rotation. Therefore, in the present study, the rotating directions of dominant vortical structures were found using streamlines in the velocity field, and the results are shown in Fig. 6 for each tip gap as viewed by an observer looking upstream. To elucidate the end-wall vortical structures, the pitchwise end-wall velocity is extracted from the velocity field. The characteristics of the flow field are visualized in the some axial planes which are approximately orthogonal to the trajectory of the tip-leakage vortex (see Fig. 5 for the locations of the planes). In Figs. 6(a)–6(c), the

locations ( $x^*/C_a$ ) of the planes are selected to show tip-clearance vortical structures at similar stages of development for different tip-gap sizes since the origins of the vortical structures vary with tip-gap size.

In general, end-wall vortical structures at similar developmental stages of the tip-leakage vortex (for example,  $x^*/C_a = 1.5$ , 1.1, and 0.7 for  $h/C_a = 6.11\%$ , 3.06%, and 1.53%, respectively) are similar for different tip-gap sizes. In the 6.11%  $C_a$  tip-gap configuration [Fig. 6(a)], the tip-leakage vortex forms at the nearly mid-chord location and develops close to the suction side of the blade tip and its size is bigger than those found in smaller tip gaps [Figs. 6(b) and 6(c)]. The induced vortex developing on the positive pitchwise side of the tip-leakage vortex appears noticeable, while the circular motion caused by the tip separation is found just underneath the blade tip. Induced vortices are found in larger numbers outside of the tip-leakage vortex in the case of 3.06% tip gap [Fig. 6(b)]. On the other hand, the tip-separation vortex is extended further in the pitchwise direction as the tip-gap size decreases. For the 1.53% tip-gap case [Fig. 6(c)], a small vortex is observed within the closed streamlines connecting the tip-leakage vortex and the tip-separation vortex. Muthanna and Devenport<sup>12</sup> performed an oil-flow visualization in the experiment with a stationary end-wall and reported the existence of the induced vortices.

The modifications of the vortical structures in their location, size, and strength are also expected to alter the cavitation pattern in the vicinity of the tip gap. From the observation in Fig. 6, potential cavitation is expected to be attached to the blade suction surface in the 6.11%  $C_a$  tip-gap configuration [Fig. 6(a)], while a sheet cavitation is more probable for the 3.06%  $C_a$  tip-gap case [Fig. 6(c)].

### C. Modification of the mean flow field and turbulence statistics

The modified vortical structures due to the tip-gap size change also suggest significant deformation of the mean flow field. Figures 7(a) and 7(b) show the contour plots of the mean streamwise velocity for three different tip gaps in the  $x$ - $y$  planes parallel to the end-wall in the locations of  $z/C_a = 0.01$  and 0.1. The streamwise velocity deficit in the cascade passage shows significant effects of the tip-gap size. At  $z/C_a = 0.01$  [Fig. 7(a)], which is inside the tip gap for all three cases, the region of low streamwise velocity develops along the pitchwise axis from the suction surface and reflects the trajectory of the tip-leakage vortex. Further away from the end-wall at  $z/C_a = 0.1$  [Fig. 7(b)], the tip-leakage deficit nearly disappears for the 1.53%  $C_a$  tip-gap, while the noticeable deficits are observed along the tip-leakage vortex in the 3.06%  $C_a$  and 6.11%  $C_a$  tip-gap simulations. In general, it is observed (not shown) that the gross magnitudes of the cross-stream velocity components decrease as the tip-gap size decreases. Compared to the magnitudes of the streamwise and pitchwise velocity components, the magnitudes of the spanwise velocity are much smaller (see Ref. 14 for the detail).

The modifications of end-wall flow structures due to the tip-gap size are also discussed in Fig. 8, which shows the mean streamwise velocity contours in the  $y$ - $z$  plane at

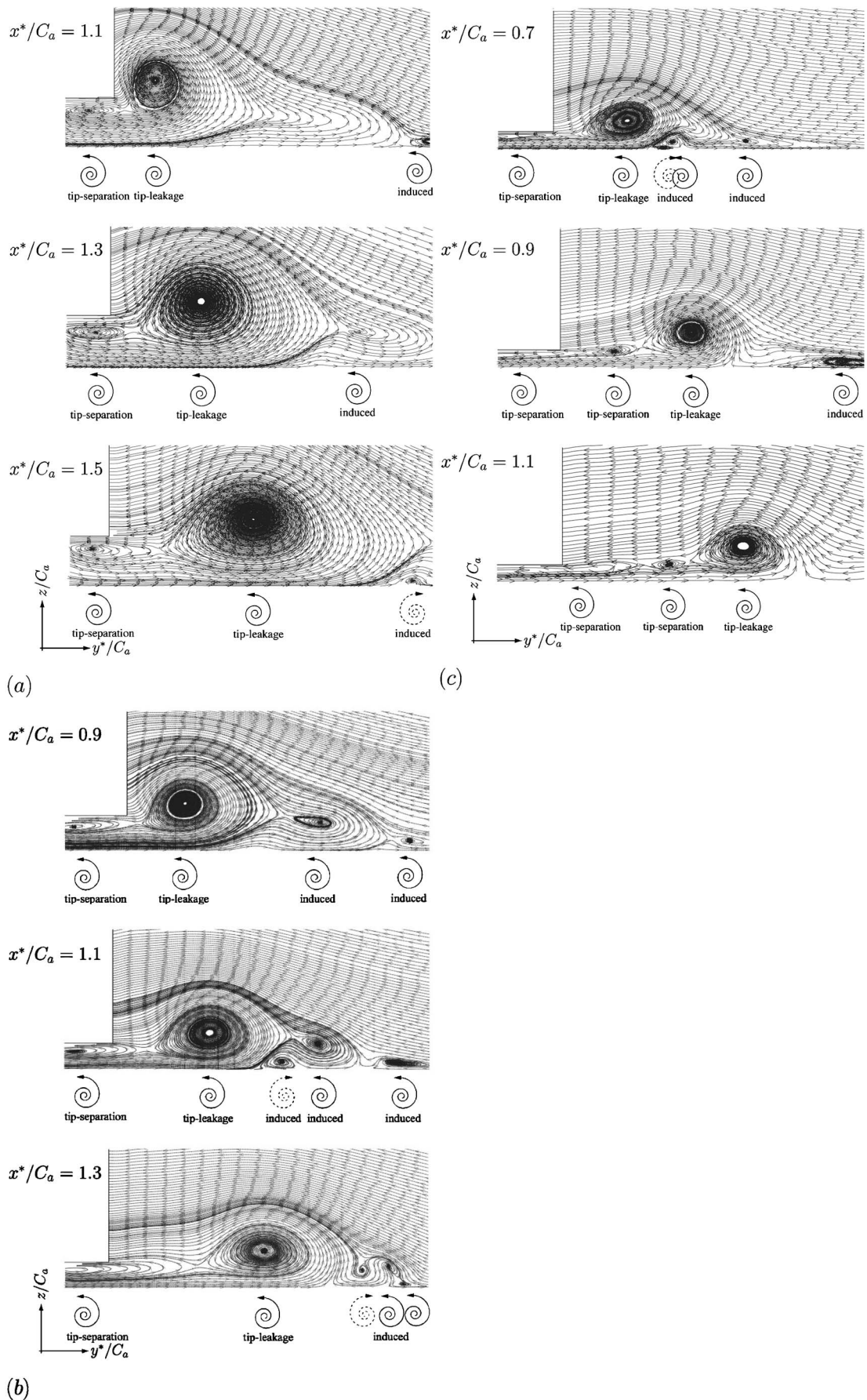


FIG. 6. Mean streamlines from three different tip-gap size simulations showing vortical structures. (a)  $h=6.11\% C_a$ ; (b)  $h=3.06\% C_a$ ; (c)  $h=1.53\% C_a$ . See Fig. 5 for the definitions and locations of the planes.

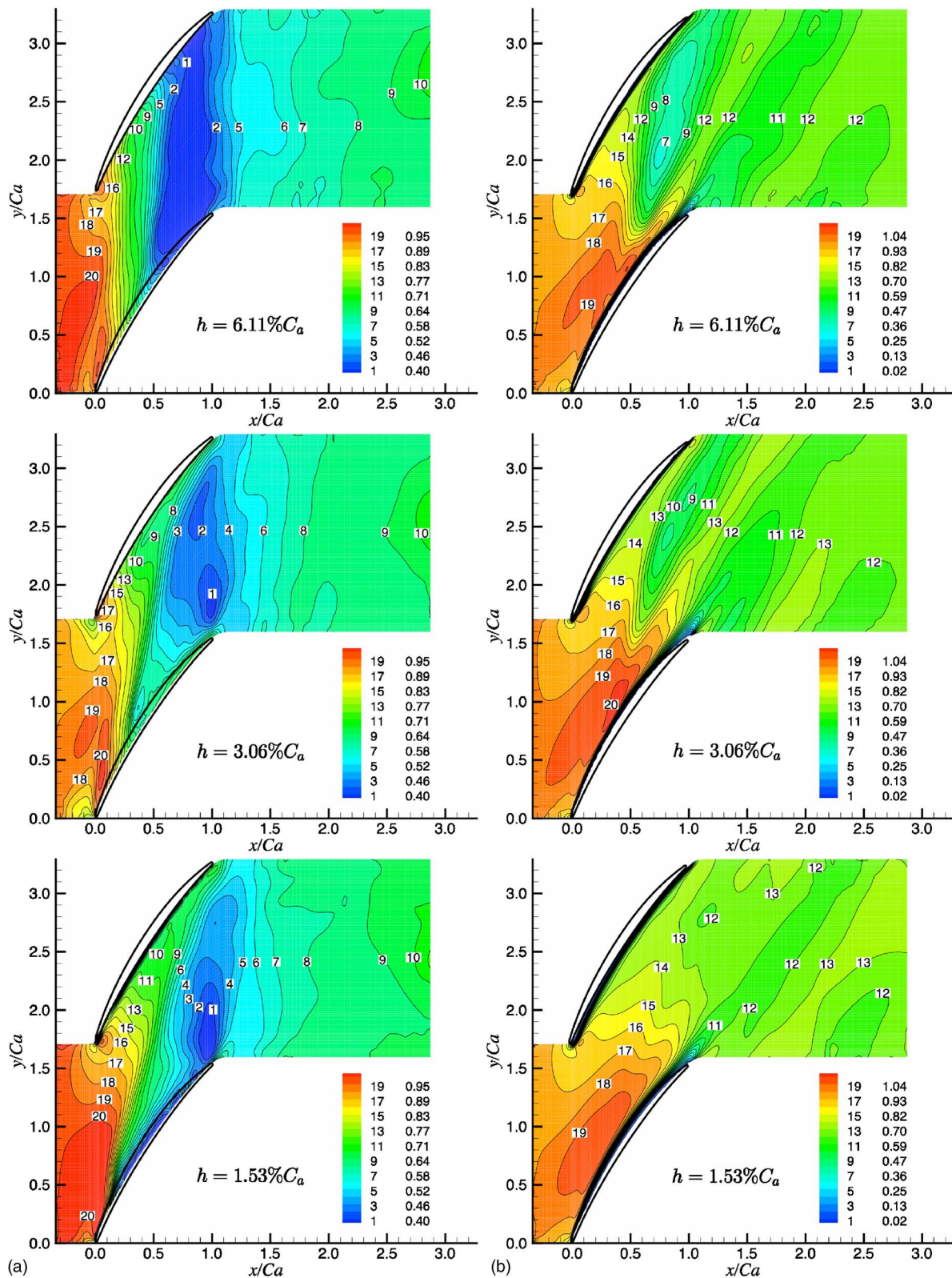


FIG. 7. Contours of mean streamwise velocity in the  $x$ - $y$  planes for three different tip-gap sizes. (a)  $z/C_a=0.01$ ; (b)  $z/C_a=0.1$ .

$x/C_a=0.6$ . Note that the definition of the present  $y$ - $z$  plane [see Fig. 1(a)] differs from those used in Figs. 5 and 6 and that Fig. 8 shows tip-leakage structures at different stages of development for different tip-gap sizes since the origins of the vortical structures vary with the tip-gap size. However, as

shown in Fig. 4, all the developed end-wall vortical structures such as the tip-leakage vortex, the tip-separation vortices, and the induced vortices are present at  $x/C_a=0.6$  in all three tip-gap cases. In the cascade passage at  $x/C_a=0.6$ , the peak streamwise velocity deficits are observed around the

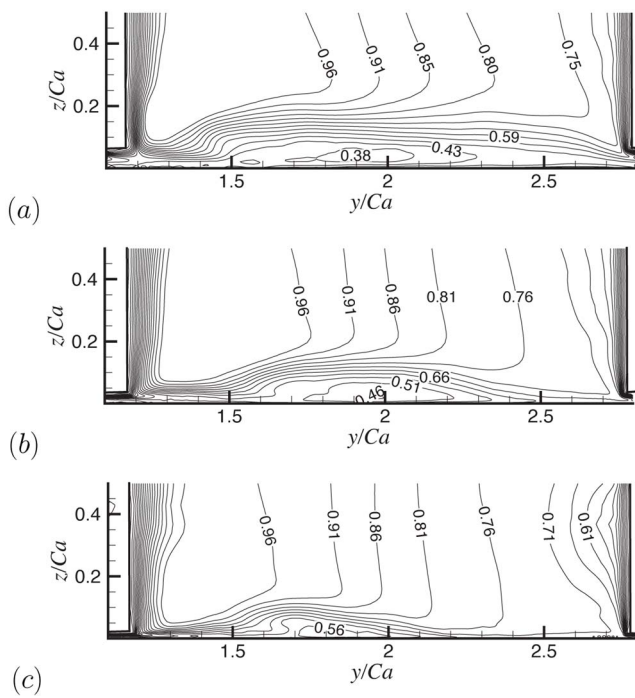


FIG. 8. Contour plots of mean streamwise velocity in the  $y$ - $z$  plane at  $x/C_a = 0.6$  for three different tip-gap sizes. (a)  $h = 6.11\% C_a$ ; (b)  $h = 3.06\% C_a$ ; (c)  $h = 1.53\% C_a$ .

tip-leakage vortex and the magnitude of the deficit is found to decrease as tip-gap size is reduced. For  $6.11\% C_a$  tip gap [Fig. 8(a)], most of the end-wall region is dominated by the streamwise velocity deficit while only about half of the end-wall region is affected by the tip-leakage vortex in the  $1.53\% C_a$  tip-gap case [Fig. 8(c)]. In terms of the streamwise velocity deficit as shown in Figs. 7 and 8, it is obvious that the smaller tip-gap size effectively reduces the strength of the tip-leakage vortex.

From the constraint for global mass conservation, the increased streamwise velocity deficit in the end-wall region increases cascade core stream velocity. In the configurations studied here, the  $1.53\% C_a$  tip-gap achieves a higher static pressure rise compared to the bigger size tip gaps due to the smaller magnitude of streamwise velocity deficit together with the smaller magnitudes of the cross-stream velocity components in the end-wall region. For this reason, a smaller tip-gap size has been preferred for axial compressors. However, for hydraulic pumps, a too small tip gap has been avoided due to the tendency for enhanced cavitation. Given that cavitation is highly correlated with the lowered pressure along the tip-leakage vortical structures, the analysis of the mean velocity field needs to be supplemented by a detailed investigation of the pressure field. An investigation of the pressure field and cavitation inception is another key objective in this study, and will be discussed in Sec. III D.

The pressure difference between the pressure and suction sides of the blade tip and the moving end-wall drives the tip-leakage flow (tip-leakage jet) across the tip gap. Figure 9 shows the pressure distribution on the blade surface near the blade tip. The pressure distribution in the tip-gap region shows a nonlinear trend with respect to the tip-gap size varia-

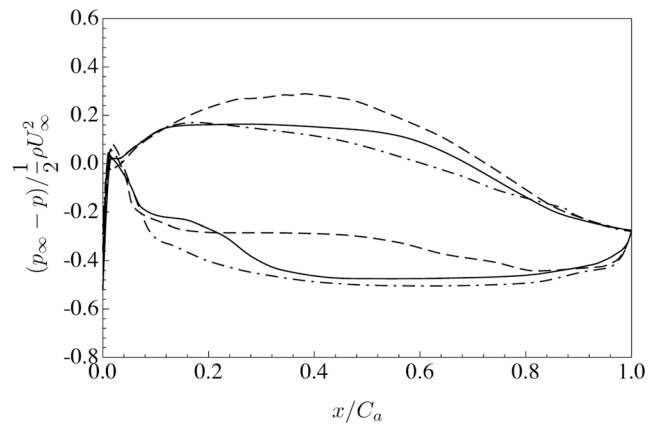


FIG. 9. Pressure distributions on the blade surface at  $0.1C_a$  away from the blade tip. ---,  $6.11\% C_a$  tip gap; —,  $3.06\% C_a$  tip gap; - · -,  $1.53\% C_a$  tip gap.

tion and is responsible for the nonlinear feature of the tip-leakage vortex propagation with respect to the tip-gap size variation as shown in Fig. 3. The streamlines in the  $3.06\% C_a$  tip-gap case in the  $x$ - $y$  planes close to the end-wall and away from the end-wall are shown in Fig. 10. A convergence of the streamlines along the locus of the tip-leakage vortex is observed in Fig. 10(a). The tip-gap flow experiences a sudden change of flow direction across the converging streamlines. Upstream of the converging streamlines, the flow direction is approximately aligned with the blade chord, while the flow direction is altered to the positive pitchwise direction in the region between the tip-leakage vortex and the blade suction surface. As a result of flow turning, the magnitude of the streamwise velocity is significantly reduced in this region as shown in Fig. 7. On the other hand, the streamlines in the  $x$ - $y$  plane away from the end-wall are aligned with the blade as shown in Fig. 10(b). The abrupt change of the streamlines along the blade span (also see Figs. 7 and 8) results in significant spanwise derivatives of the streamwise and pitchwise velocity components ( $\partial U/\partial z$  and  $\partial V/\partial z$ ). In Ref. 14, it was reported that the large spanwise derivatives of the streamwise and pitchwise velocity components are the major sources of strong vorticity and turbulent kinetic energy production.

Altering the tip-gap size modifies the vorticity field as shown in Figs. 11 and 12. For all three tip gaps, the streamwise (Fig. 11) and pitchwise (Fig. 12) vorticity components dominate the end-wall vorticity field while the contribution of the spanwise vorticity (not shown) is noticeable only in the blade boundary layer. This is related to the large spanwise derivatives of the streamwise and pitchwise velocity components in the leakage flow as aforementioned:  $\Omega_x = 1/2(\partial W/\partial y - \partial V/\partial z) \approx -1/2(\partial V/\partial z)$  and  $\Omega_y = 1/2(\partial U/\partial z - \partial W/\partial x) \approx 1/2(\partial U/\partial z)$ . The comparison of the vorticity fields in Figs. 11 and 12 implies that the mechanism for the vorticity generation is mostly unchanged by tip-gap size variation. In general, the peak magnitudes of the streamwise and pitchwise vorticity components in the tip-leakage vortex are found to be reduced as the tip-gap size decreases.

The spanwise derivatives of the streamwise and pitchwise velocity components are also responsible for turbulent

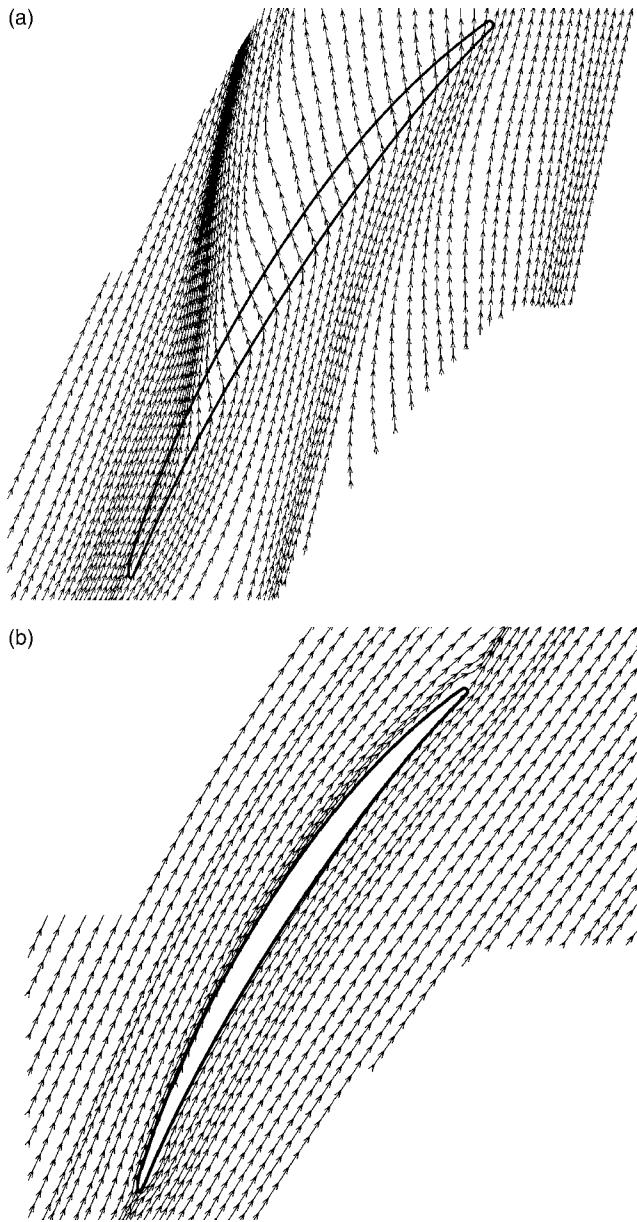


FIG. 10. Mean streamlines in the 3.06%  $C_a$  tip-gap case in the  $x$ - $y$  planes. (a)  $z/C_a=0.025$ ; (b)  $z/C_a=0.5$ .

kinetic energy production. The production term in the transport equation for the turbulent kinetic energy is decomposed into

$$\begin{aligned} \varphi = & \underbrace{-\overline{u'u'}}_{\varphi_1} \frac{\partial U}{\partial x} - \underbrace{\overline{v'v'}}_{\varphi_2} \frac{\partial V}{\partial y} - \underbrace{\overline{w'w'}}_{\varphi_3} \frac{\partial W}{\partial z} - \underbrace{\overline{u'v'}}_{\varphi_4} \left( \frac{\partial U}{\partial y} + \frac{\partial V}{\partial x} \right) \\ & - \underbrace{\overline{u'w'}}_{\varphi_5} \left( \frac{\partial U}{\partial z} + \frac{\partial W}{\partial x} \right) - \underbrace{\overline{v'w'}}_{\varphi_6} \left( \frac{\partial V}{\partial z} + \frac{\partial W}{\partial y} \right). \end{aligned} \quad (1)$$

In the all three tip-gap simulations, it is found that the turbulent kinetic energy production in the end-wall region is dominated by the  $\varphi_5$  and  $\varphi_6$  terms which are associated with the large spanwise derivatives of the streamwise and pitch-

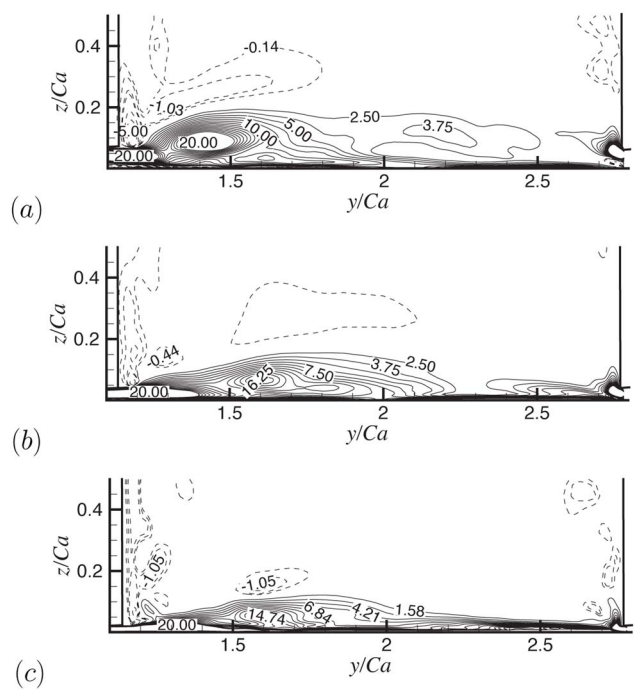


FIG. 11. Contour plots of mean streamwise vorticity in the  $y$ - $z$  plane at  $x/C_a=0.6$  for three different tip-gap sizes. (a)  $h=6.11\% C_a$ ; (b)  $h=3.06\% C_a$ ; (c)  $h=1.53\% C_a$ .

wise velocity components ( $\partial U/\partial z$  and  $\partial V/\partial z$ ). In Fig. 13, the effects of tip-gap size on the mean turbulent kinetic energy are examined in the  $y$ - $z$  plane at  $x/C_a=0.6$ . In general, high levels of the turbulent kinetic energy are concentrated in the regions of the tip-leakage vortex and tip-leakage jet, and the

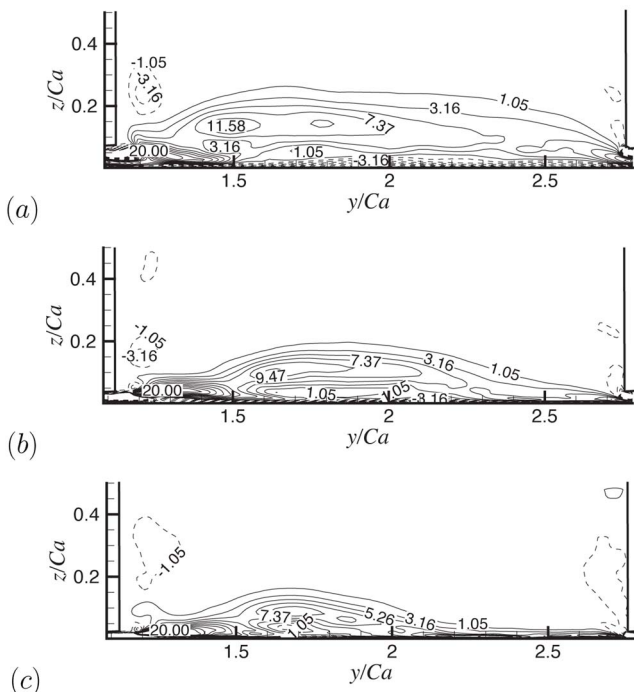


FIG. 12. Contour plots of mean pitchwise vorticity in the  $y$ - $z$  plane at  $x/C_a=0.6$  for three different tip-gap sizes. (a)  $h=6.11\% C_a$ ; (b)  $h=3.06\% C_a$ ; (c)  $h=1.53\% C_a$ .

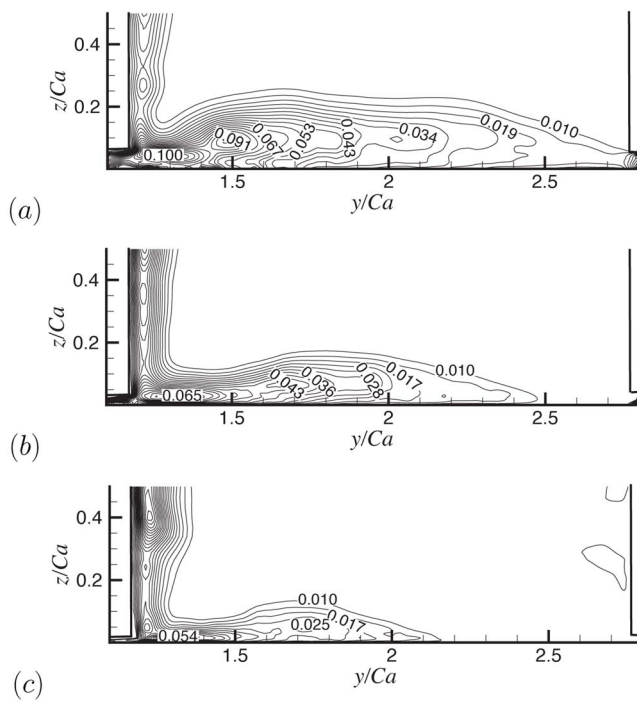


FIG. 13. Contour plots of mean turbulent kinetic energy in the  $y$ - $z$  plane at  $x/C_a = 0.6$ . (a)  $h = 6.11\% C_a$ ; (b)  $h = 3.06\% C_a$ ; (c)  $h = 1.53\% C_a$ .

size of these regions is found to increase with the tip gap. The magnitude of the mean turbulent kinetic energy is observed to decrease when the tip-gap size is reduced. Therefore, the viscous losses associated with the tip-clearance flow in terms of the magnitudes of vorticity and turbulent kinetic energy are found to be reduced as the tip-gap size decreases (Figs. 11–13). The magnitudes of the Reynolds stresses (not shown) are observed to be reduced as the tip-gap size decreases. However, the distribution and relative magnitudes of Reynolds stresses are observed to be qualitatively unaltered by changing the tip-gap size. This suggests that the underlying mechanisms for the production of the turbulent fluctuations are also unchanged with the tip-gap size variation (see Ref. 14 for detailed analysis of the turbulent kinetic energy and its production in the  $3.06\% C_a$  tip-gap configuration).

#### D. Effects on the pressure and cavitation

The modified tip-leakage vortex also changes mean pressure and pressure fluctuations in the vicinity of the tip gap. The mean pressure distributions in the  $x$ - $y$  plane for each tip gap are compared in Fig. 14. The low-pressure is concentrated in the region of the tip-leakage vortex, the tip-leakage jet region, and underneath the blade tip. The general shape of the low pressure region also represents the gross features of the tip-leakage vortex. As expected from the analysis of the mean velocity field (Sec. III C), the downstream pressure is observed to increase as the tip-gap size decreases, while the peak magnitude of negative pressure is found to increase with tip gap. From this perspective, it is confirmed that in the present linear cascade configuration, the  $1.53\% C_a$  tip-gap

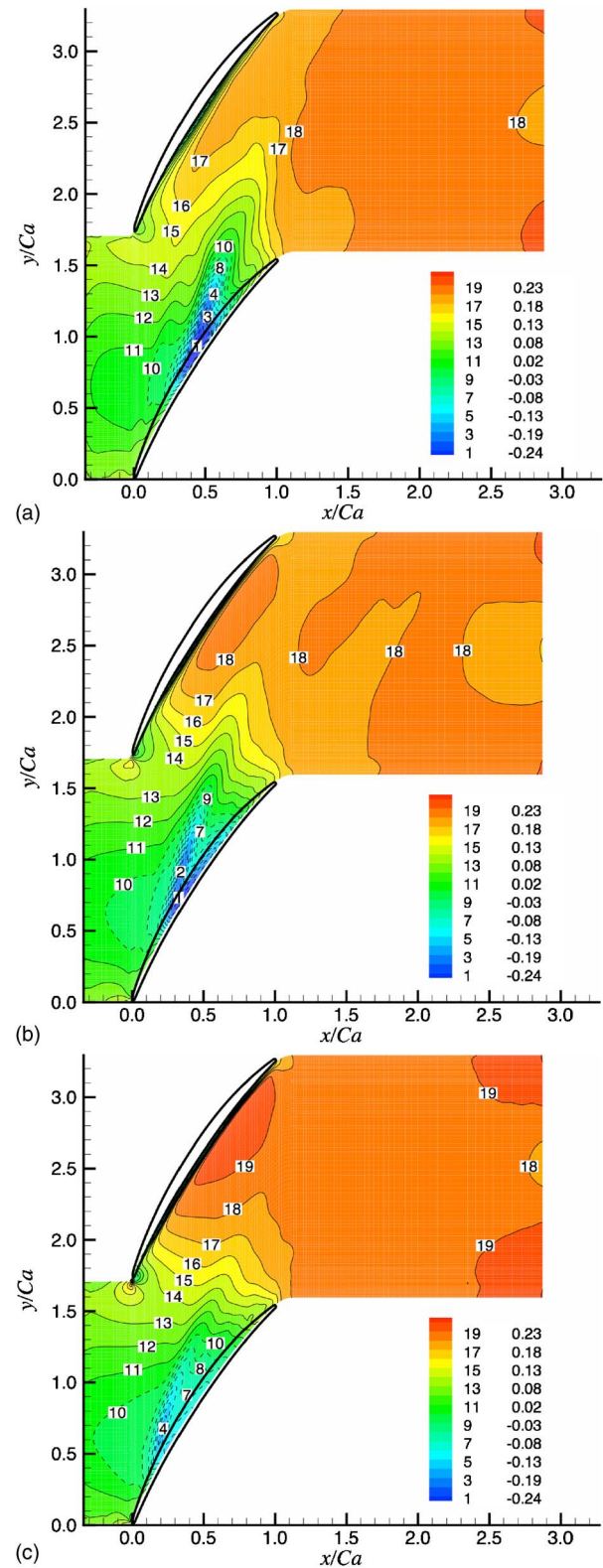


FIG. 14. Contour plots of mean pressure in the  $x$ - $y$  plane at  $z = 0.01 C_a$  for three different tip-gap sizes. (a)  $h = 6.11\% C_a$ ; (b)  $h = 3.06\% C_a$ ; (c)  $h = 1.53\% C_a$ .

performs better for achieving a higher static pressure rise in the cascade exit. In addition, the cavitation inception index is expected to increase with the tip-gap size.

The highly unsteady vortical motions also produce in-

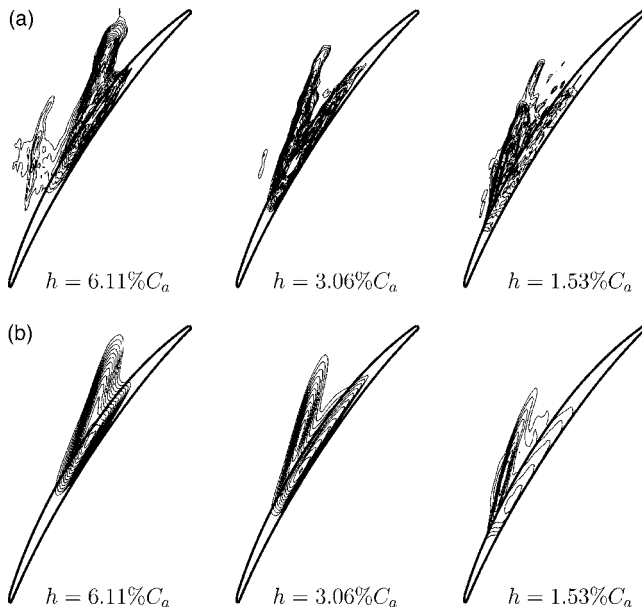


FIG. 15. (a) Instantaneous and (b) time-averaged contours of cavitation stress ( $B$ ) in the  $x$ - $y$  plane at  $z=0.01C_a$  for three different tip-gap sizes.

tense pressure fluctuations around the vortices. As observed in other flow quantities such as mean streamwise velocity, vorticity, and turbulent kinetic energy (see Sec. III C), the region of high level of pressure fluctuations is also found to increase in size with tip gap. Pressure fluctuations play an important role in triggering cavity bubbles, especially in the region where the mean pressure is close to the critical vapor pressure.

Understanding the distribution of negative pressure and pressure fluctuations is important in analyzing and predicting the cavitation phenomenon. The pressure fields obtained from the present LES are analyzed in order to elucidate the mechanisms responsible for low-pressure events and cavitation inception. It is generally difficult to accurately predict cavitation using single-phase CFD,<sup>25,26</sup> although a variety of cavitation-inception criteria have been developed.<sup>25,27,28</sup> In this analysis, the one proposed by Joseph,<sup>28</sup> which consists of the local pressure, vapor pressure, and tensile stress of the fluid is applied.

Figure 15 shows an example of cavitation inception analysis using the minimum tension criterion proposed by Joseph.<sup>28</sup> This criterion is based on the normal stress of the fluid and the critical vapor pressure:

$$B_{ii} = \tau_{ii} - p + p_c > 0, \quad (2)$$

where  $\tau_{ii}$  is the normal stress,  $p$  is local pressure, and  $p_c$  is the pressure in the cavity. For this example,  $p_c/\rho U_\infty^2$  of 0.01 is used, assuming a cavitation number of 0.02 based on the cascade inlet pressure. If all three components of the stress  $B_{11}$ ,  $B_{22}$ , and  $B_{33}$  are positive, a cavity will open. Similar discussions can be found in Knapp *et al.*<sup>27</sup>

Instantaneous and time-averaged isosurfaces and contours of  $B=1/3(B_{11}+B_{22}+B_{33})$  are plotted in Fig. 15, in regions where all three components are positive. High levels of  $B$  in both the instantaneous and time-averaged contours are concentrated in the tip-leakage region. In particular, the tip-

leakage vortex appears as the dominant source of cavitation in these plots. For the 6.11%  $C_a$  tip-gap case, the induced vortex is found to lead to a potential cavitation region based on some instantaneous pressure fields. In this case, the cavitation associated with the tip-leakage vortex can be classified as attached cavitation since it is attached to the suction surface of the blade (Fig. 15,  $h=6.11\% C_a$ ). For the 3.06%  $C_a$  tip gap, two distinct regions of potential cavitation are found along the tip-leakage vortex and underneath the blade tip. The cavitation along the tip-leakage vortex can be best defined as tip-leakage vortex cavitation (Fig. 15,  $h=3.06\% C_a$ ). If the tip-gap size is reduced to 1.53%  $C_a$ , the cavitating tip-leakage vortex is connected to the blade by the tip-leakage jet which may also cavitate. In this sense, the cavitation phenomenon in the 1.53%  $C_a$  tip-gap case could be described as a sheet cavitation (Fig. 15).

The present results also suggest that the 1.53%  $C_a$  tip-gap is better for minimizing the tip-leakage vortex and the resulting cavitation. Farrell and Billet<sup>6</sup> found that a minimum cavitation inception index exists when the ratio of tip-gap size to the maximum tip thickness ( $\delta$ ) is in a certain range. Their correlation and existing experimental data employing axial-flow pumps indicate that a range of  $\delta \approx 0.1-0.2$  achieves minimum cavitation indices. Both bigger and smaller values of  $\delta$  were found to increase the cavitation inception index. Considering that, in the present study,  $\delta_s$  are 0.11, 0.22, and 0.43 for the tip-gap sizes of 1.53%  $C_a$ , 3.06%  $C_a$ , and 6.11%  $C_a$ , respectively, the present results are consistent with the finding of Farrell and Billet.<sup>6</sup> However, it is unclear whether the tip-gap size around 1.53%  $C_a$  is optimal for minimizing tip-leakage cavitation in the present configuration. For a very large tip-gap, the cavitation inception index is expected to decrease due to the reduced strength of the tip-leakage vortex. However, in the present LES and Farrell and Billet's experiments,<sup>6</sup> it is unclear what is the tip-gap size for the peak cavitation inception index.

#### IV. CONCLUSIONS

Tip-gap size is one of the most important parameters which determine the various features of the tip-clearance flow in turbomachines. In this study, LES results for three tip gaps of 6.11%  $C_a$ , 3.06%  $C_a$ , and 1.53%  $C_a$  in a linear cascade with moving end-wall have been analyzed in order to understand the effects of tip-gap size on the end-wall vortex dynamics, mean flow and turbulence statistics, and tip-leakage cavitation.

Considering that the tip-leakage vortex as well as the induced and tip-separation vortices are closely related to the generation of tip-leakage cavitation and its propagation pattern, the effects of tip-gap size on the generation and evolution of the end-wall vortical structures have been extensively discussed. For all three tip gaps considered in this study, the tip-leakage vortex is found to dominate the end-wall vortical structures. The size of the tip-leakage vortex increases with the tip-gap size while its origin is delayed further downstream. The angle between the blade chord and the tip-leakage vortex also increases with the tip-gap size. Although the propagation path of the tip-leakage vortex shows strong

variation with the tip-gap size in the cascade passage, it is nearly independent of the tip-gap size in the downstream of the cascade. Since the tip-leakage vortex is lifted from the end-wall in the downstream, the vortex convects following the cascade main stream and the resulting angle of vortex propagation becomes similar to that of the blade wake. In contrast to the lifted tip-leakage vortex, the tip-separation vortices are driven by both the end-wall motion and the cascade main stream and results in a higher propagation angle than that of the tip-leakage vortex. Induced vortices are observed to be strong in the bigger tip gap, while the tip-separation vortices are enhanced in both numbers and strengths as the tip-gap size decreases.

The peak streamwise velocity deficit and magnitudes of vorticity and turbulent kinetic energy, and associated viscous losses are reduced as the tip-gap size decreases. Significant levels of streamwise and pitchwise vorticity components and turbulent fluctuations are found in the region of tip-leakage jet and tip-leakage vortex. This is related to the large spanwise derivatives of the streamwise and pitchwise velocity components in the tip-leakage flow, and these derivatives are also responsible for turbulent kinetic energy production. The present observation implies that the mechanism for the generation of vorticity and turbulent kinetic energy is mostly unchanged by the tip-gap size variation.

The modified tip-leakage vortex due to the tip-gap size variation is found to significantly change the mean pressure and pressure fluctuations in the vicinity of the tip gap. Low-pressure and pressure fluctuations are concentrated in the regions of the tip-leakage vortex and tip-leakage jet. Based on this, it is suggested that, for the three tip gaps considered, tip-leakage cavitation is enhanced as the tip-gap size increases. In addition, it is confirmed that the smallest tip-gap size performs best in achieving a static pressure rise in the cascade exit.

In this study, the cascade with 1.53%  $C_a$  tip gap is found to be better in minimizing the tip-leakage vortex and the resulting cavitation than the cascades with bigger tip gaps. However, it is unclear whether this is the optimal tip-gap size for minimizing tip-leakage cavitation. In addition, the present linear cascade configuration lacks some important features which exist in actual hydraulic pumps. Rotating effect is one of the missing factors which can alter the cavitation phenomenon.

The present study suggests that the fundamental features of the tip-clearance flow are not altered by the different tip-gap sizes. Therefore, the guidelines for controlling tip-leakage cavitation and viscous losses which can be deduced from an analysis of the velocity and pressure fields are expected to be effective for the various tip-gap sizes. In addition, the present results suggest that the potential of combining control methodology with a tip-gap optimization to achieve better tip-leakage cavitation control.

## ACKNOWLEDGMENTS

The authors acknowledge the support of the Office of Naval Research under Grant No. N00014-99-1-0389, with Dr. Ki-Han Kim as the program manager. Computer time

was provided by a Challenge Project Grant (C82) from the U.S. Department of Defense (DoD) High Performance Computing Modernization Program (HPCMP) through the Army Research Laboratory (ARL) Major Shared Resource Center (MSRC). The authors would also like to thank Professor William Devenport of VPI for providing his experimental data.

- <sup>1</sup>M. Furukawa, K. Saiki, K. Nagayoshi, M. Kuroamaru, and M. Inoue, "Effects of stream surface inclination on tip leakage flow fields in compressor rotors," *J. Turbomach.* **120**, 683 (1998).
- <sup>2</sup>R. Mailach, I. Lehmann, and K. Vogeler, "Rotating instabilities in an axial compressor originating from the fluctuating blade tip vortex," *J. Turbomach.* **123**, 453 (2001).
- <sup>3</sup>K. L. Suder, "Blockage development in a transonic, axial compressor rotor," *J. Turbomach.* **120**, 465 (1998).
- <sup>4</sup>W. C. Zierke, K. J. Farrell, and W. A. Straka, "Measurement of the tip clearance flow for a high-Reynolds-number axial-flow rotor," *J. Turbomach.* **117**, 522 (1995).
- <sup>5</sup>W. C. Zierke and W. A. Straka, "Flow visualization and the three-dimensional flow in an axial flow pump," *J. Propul. Power* **12**, 250 (1996).
- <sup>6</sup>K. J. Farrell and M. L. Billet, "A correlation of tip leakage vortex cavitation in axial-flow pumps," *J. Fluids Eng.* **116**, 551 (1994).
- <sup>7</sup>O. Boulon, M. Callenaere, J. P. Franc, and J. M. Michel, "An experimental insight into the effect of confinement on tip vortex cavitation of an elliptical hydrofoil," *J. Fluid Mech.* **390**, 1 (1999).
- <sup>8</sup>S. Gopalan, J. Katz, and H. L. Liu, "Tip leakage cavitation, associated bubble dynamics, noise, flow structure and effect of tip gap size," CAV2001: Fourth International Symposium on Cavitation, 2001.
- <sup>9</sup>M. Inoue, M. Kuroamaru, and M. Fukuhara, "Behavior of tip-leakage flow behind an axial compressor rotor," *J. Eng. Gas Turbines Power* **108**, 7 (1986).
- <sup>10</sup>A. Goto, "Three-dimensional flow and mixing in an axial flow compressor with different rotor tip clearance," *J. Turbomach.* **114**, 675 (1992).
- <sup>11</sup>J. A. Storer and N. A. Cumpsty, "Tip leakage flows in axial compressors," ASME Paper No. 90-GT-127, 1990.
- <sup>12</sup>C. Muthanna and W. J. Devenport, "Wake of a compressor cascade with tip gap. Part 1. Mean flow and turbulence structure," *AIAA J.* **42**, 2320 (2004).
- <sup>13</sup>Y. Wang and W. J. Devenport, "Wake of a compressor cascade with tip gap. Part 2. Effects of endwall motion," *AIAA J.* **42**, 2332 (2004).
- <sup>14</sup>D. You, P. Moin, M. Wang, and R. Mittal, "Study of tip clearance flow in a turbomachinery cascade using large eddy simulation," Report No. TF-86, Department of Mechanical Engineering, Stanford University, Stanford, California, May 2004.
- <sup>15</sup>S. Shin, "Reynolds-averaged Navier-Stokes computation of tip-clearance flow in a compressor cascade using an unstructured grid," Ph.D. thesis, Department of Aerospace and Ocean Engineering, Virginia Polytechnic Institute and State University, Blacksburg, Virginia, September 2001.
- <sup>16</sup>M. R. Khorrami, F. Li, and M. Choudhan, "Novel approach for reducing rotor tip-clearance-induced noise in turbofan engines," *AIAA J.* **40**, 1518 (2002).
- <sup>17</sup>D. You, R. Mittal, M. Wang, and P. Moin, "Computational methodology for large-eddy simulation of tip-clearance flows," *AIAA J.* **42**, 271 (2004).
- <sup>18</sup>C. Meneveau, T. S. Lund, and W. H. Cabot, "A Lagrangian dynamic subgrid-scale model of turbulence," *J. Fluid Mech.* **319**, 233 (1996).
- <sup>19</sup>T. S. Lund, X. Wu, and K. D. Squires, "Generation of turbulent inflow data for spatially developing boundary layer simulations," *J. Comput. Phys.* **140**, 233 (1998).
- <sup>20</sup>D. You, M. Wang, R. Mittal, and P. Moin, "Large-eddy simulations of longitudinal vortices embedded in a turbulent boundary layer," *AIAA J.* (to be published).
- <sup>21</sup>D. You, R. Mittal, M. Wang, and P. Moin, "Large-eddy simulation of a rotor tip-clearance flow," AIAA Paper No. 2002-0981, 2002.
- <sup>22</sup>D. You, R. Mittal, M. Wang, and P. Moin, "Analysis of stability and accuracy of finite-difference schemes on a skewed mesh," *J. Comput. Phys.* **213**, 184 (2006).
- <sup>23</sup>K. Akselvoll and P. Moin, "Large eddy simulation of turbulent confined

- coannular jets and turbulent flow over a backward facing step,” Report No. TF-63, Department of Mechanical Engineering, Stanford University, Stanford, California, February 1995.
- <sup>24</sup>J. Jeong and F. Hussain, “On the identification of a vortex,” *J. Fluid Mech.* **285**, 69 (1995).
- <sup>25</sup>R. E. A. Arndt, “Cavitation in fluid machinery and hydraulic structures,” *Annu. Rev. Fluid Mech.* **13**, 273 (1981).
- <sup>26</sup>I. Senocak, “Computational methodology for the simulation of turbulent cavitating flows,” Ph.D. thesis, Department of Mechanical Engineering, University of Florida, Gainesville, Florida, 2000.
- <sup>27</sup>R. T. Knapp, J. W. Daily, and F. G. Hammitt, *Cavitation* (McGraw-Hill, New York, 1970).
- <sup>28</sup>D. D. Joseph, “Cavitation and the state of stress in a flowing liquid,” *J. Fluid Mech.* **366**, 367 (1998).